CHEMISTRY OF MATERIALS
Article

Chem. Mater. **2010,** *22,* 6221–6228 6221
DOI:10.1021/cm1021432

^{29}Si and ^{13}C Solid-State NMR Spectroscopic Study of Nanometer-Scale Structure and Mass Fractal Characteristics of Amorphous Polymer Derived Silicon Oxycarbide Ceramics

S. J. Widgeon,[†] S. Sen,*[,†] G. Mera,[§] E. Ionescu,[§] R. Riedel,[§] and A. Navrotsky[†,‡]

[†]*Department of Chemical Engineering and Materials Science, and* [‡]*Peter A. Rock Thermochemistry Laboratory and NEAT ORU, University of California at Davis, Davis, California 95616, United States, and* [§]*Technische Universität Darmstadt, Institut für Materialwissenschaft, Petersenstrasse 23, D-64287 Darmstadt, Germany*

Received May 14, 2010. Revised Manuscript Received October 15, 2010

Polymer derived silicon oxycarbide ceramics (SiOC-PDCs) with widely different carbon contents have been synthesized, and their structures have been studied at different length scales using high-resolution ^{13}C and ^{29}Si magic-angle-spinning (MAS) NMR spectroscopic techniques. The data suggest that the structure of these PDCs consists of a continuous mass fractal backbone of corner-shared SiC_xO_{4-x} tetrahedral units with "voids" occupied by sp^2-hybridized graphitic carbon. The oxygen-rich SiC_xO_{4-x} units are located at the interior of this backbone with a mass fractal dimension of ~2.5 while the carbon-rich units display a slightly lower dimensionality and occupy the interface between the backbone and the free carbon nanodomains.

Introduction

Amorphous polymer derived silicon oxycarbide ceramics (SiOC-PDCs) belong to a new class of materials that are X-ray amorphous but display structural heterogeneity at the nanometer length scale.[1,2] These materials can be synthesized by careful thermal decomposition of Si-based preceramic polymers which provide silicon, carbon, and oxygen (or nitrogen and/or boron for ceramics in the Si−B−C−N system) in controlled proportions. These materials are lightweight, have excellent mechanical properties, and are stable against crystallization, oxidation, and corrosion up to temperatures near 1800 K.[3−10] Recent calorimetric studies have shown that SiOC-PDCs are thermodynamically stable with respect to an isocompositional mixture of cristobalite, silicon carbide, and graphite.[11] Moreover, their properties can be tuned over a wide range by controlling the relative ratios of the constituent elements.[1,2]

Fundamental understanding of the atomic structure of SiOC-PDCs is critical in deciphering the structure−property relationships in these materials and ultimately in controlling their properties for specific engineering applications. The atomic structure of these materials has, therefore, been extensively investigated over the last two decades using a wide variety of spectroscopic, scattering, and electron microscopic techniques.[12−25] It is generally agreed that

*To whom correspondence should be addressed. Tel.: 1(530)754-8397. Fax:1(530)752-1031.

(1) Pantano, C. G; Singh, A. T.; Zhang, H. *J. Sol-Gel Sci. Technol.* **1999**, *14*, 7.
(2) Riedel, R.; Mera, G.; Hauser, R.; Klonczynski, A. *J. Ceram. Soc. Jpn.* **2006**, *114*, 425.
(3) Rouxel, T.; Soraru, G. D.; Vicens, J. *J. Am. Ceram. Soc.* **2001**, *84*, 1052.
(4) Soraru, G. D.; Modena, S.; Guadagnino, E.; Colombo, P.; Egan, J.; Pantano, P. *J. Am. Ceram. Soc.* **2002**, *85*, 1529.
(5) Soraru, G. D.; Modena, S.; Bettotti, P.; Das, G.; Mariotto, G.; Pavesi, L. *Appl. Phys. Lett.* **2003**, *83*, 749.
(6) Scarmi, A.; Soraru, G. D.; Raj, R. *J. Non-Cryst. Solids* **2005**, *351*, 2238.
(7) Rouxel, T.; Massouras, G.; Soraru, G. D. *J. Sol-Gel Sci. Technol.* **1999**, *14*, 87.
(8) Bois, L.; Maquet, J.; Babonneau, F.; Mutin, H.; Hahloul, D. *Chem. Mater.* **1995**, *7*, 975.
(9) Weinmann, M.; Schumacher, J.; Kummer, H.; Prinz, S.; Peng, J.; Seifert, H. J.; Christ, M.; Müller, K.; Bill, J.; Aldinger, F. *Chem. Mater.* **2000**, *12*, 623.
(10) Wang, Z. C.; Aldinger, F.; Riedel, R. *J. Am. Ceram. Soc.* **2001**, *84*, 2179.
(11) Varga, T.; Navrotsky, A.; Moats, J.; Morcos, R.; Poli, F.; Muller, K.; Saha, A.; Raj, R. *J. Am. Ceram. Soc.* **2007**, *90*, 3213.
(12) Bois, L.; Maquet, J.; Babonneau, F.; Mutin, H.; Hahloul, D. *Chem. Mater.* **1994**, *6*, 796.
(13) Corriu, R. J. P.; Leclerco, D.; Mutin, P. H.; Vioux, A. *J. Sol-Gel Sci. Technol.* **1997**, *8*, 327.
(14) Soraru, G. D.; D'Andrea, G.; Campostrini, R.; Babonneau, F.; Mariotto, G. *J. Am. Ceram. Soc.* **1995**, *78*, 379.
(15) Kleebe, H. J.; Turquat, C.; Sorau, G. C. *J. Am. Ceram. Soc.* **2001**, *84*, 1073.
(16) Gregori, G.; Turquat, C.; Kleebe, H. J.; Soraru, G. D. *Key Eng. Mater.* **2002**, *206−213*, 2061–2064.
(17) Saha, A.; Raj, R.; Williamson, D. L.; Kleebe, H. J. *J. Am. Ceram. Soc.* **2005**, *88*, 232.
(18) Brequel, H.; Parmentier, J.; Walter, S.; Badheka, R.; Trimmel, G.; Masse, S.; Latournerie, J.; Dempsey, P.; Turquat, C.; Desmartin-Chomel, A.; Le Neindre-Prum, L.; Jayasooriya, U. A.; Hourlier, D.; Kleebe, H. J.; Soraru, G. D.; Enzo, S.; Babonneau, F. *Chem. Mater.* **2004**, *16*, 2585.
(19) Gabriel, A. O.; Riedel, R.; Dressler, W.; Reichert, S.; Gervais, C.; Maquet, J.; Babonneau, F. *Chem. Mater.* **1999**, *11*, 412.
(20) Turquat, C.; Kleebe, H. J.; Gregori, G.; Walter, S.; Soraru, G. D. *J. Am. Ceram. Soc.* **2001**, *84*, 2189.
(21) Saha, A.; Raj, R.; Williamson, D. L. *J. Am. Ceram. Soc.* **2006**, *89*, 2188.
(22) Corriu, R. J. P.; Leclerco, D.; Mutin, P. H.; Vioux, A. *J. Mater. Sci.* **1995**, *30*, 2313.
(23) Kleebe, H. J.; Blim, Y. D. *J. Eur. Ceram. Soc.* **2008**, *28*, 1037.
(24) Trimmel, G.; Rita, B.; Babonneau, F.; Latournerie, J.; Dempsey, P.; Bahloul-Houlier, D.; Parmentier, J.; Soraru, G. D. *J. Sol-Gel Sci. Technol.* **2003**, *26*, 279.
(25) Burns, G. T.; Taylor, R. B.; Xu, Y.; Zangvil, A.; Zank, G. A. *Chem. Mater.* **1992**, *4*, 1313.

Published on Web 11/10/2010

the short-range structure of these materials contains silicon atoms forming SiC_xO_{4-x} tetrahedra where $0 \geq x \geq 4$. However, very little is known about the spatial distribution and connectivity between these tetrahedral units at length scale of the next-nearest neighbors and beyond. Previous structural studies have also shown that besides bonding to silicon atoms, some carbon atoms are also bonded to other carbon atoms, although carbon−oxygen bonding in the structure is excluded.[1,2] Results from ^{29}Si nuclear magnetic resonance (NMR), electron energy loss (EELS), and Raman spectroscopic studies have provided evidence of excess or "free" carbon in these materials that form nanodomains of sp^2-bonded carbon, presumably present as turbostratic carbon or as graphene-like sheets.[1] However, the morphology and characteristic length scale of these nanodomains remain largely unknown and highly controversial. One of the original proposals (referred to hereafter as model 1) was a scenario where the free carbon is present in approximately spherical nanodomains or as dispersed graphene and/or turbostratic graphite segments embedded in a matrix that is a network of interconnected SiC_xO_{4-x} tetrahedra.[15,20,21] Recently, a second structural model (referred to hereafter as model 2) has been proposed on the basis of small-angle X-ray scattering (SAXS) studies and observations of high-creep resistance.[17,21] According to this model, the structure of SiCO ceramics consists of a cellular network of interconnected graphene sheets or turbostratic carbon with silica-rich nanodomains sequestered within the cells. The domain walls that connect the graphene sheets to the silica consist primarily of carbon-rich SiC_xO_{4-x} tetrahedra. For each model, the characteristic length scale of the nanodomains was proposed to be on the order of a few nanometers. Specifically, in model 2, the SAXS measurements suggested that the silica-rich domains ranged in diameter from 1 to 5 nm while the widths of the domain walls composed of carbon-rich SiC_xO_{4-x} tetrahedra were found to range from 0.8 to1.5 nm.

The nature of the structural heterogeneity in amorphous materials at the nanometer length scale is crucial in understanding a wide range of phenomena including ionic conduction, nucleation, and crystallization and mechanical properties such as creep and viscoelasticity. However, structural studies of amorphous materials such as SiOC-PDCs at length scales beyond the next-nearest neighbors are not straightforward, as most spectroscopic techniques are sensitive to shorter ranges ($\leq$0.5 nm). Previous studies of amorphous materials have shown that nuclear spin−lattice relaxation spectroscopy can be used quite effectively to investigate the spatial distribution of nuclides in specific atomic environments, particularly when the relaxation of the nuclear spins is controlled by temporal fluctuation of direct dipolar coupling to free electronic spins in paramagnetic impurities (e.g., transition metal and/or rare earth ions) or defects in the form of dangling bonds in the structure.[26−28] Such impurities or defects are typically present in a material at concentration levels of few tens to hundreds of parts per million (ppm) and either are originally present in the reactants used for synthesis or get introduced during processing. This scenario of nuclear spin−lattice relaxation has been demonstrated to be valid for the spin−lattice relaxation of spin $I = 1/2$ nuclides such as ^{29}Si in solids where any internuclear dipolar coupling and nuclear spin diffusion are negligible. This is indeed the case for SiOC-PDCs where the natural abundances of the NMR active nuclides ^{29}Si, ^{13}C, and ^{17}O are quite small (4.7%, 1.1%, and 0.04%, respectively).

In the case of nuclear spin−lattice relaxation caused by direct dipolar coupling to free electronic spins in paramagnetic impurities or defects, the time dependence of the recovered magnetization $M(t)$ display a complex non-exponential relaxation behavior that can be divided into three regimes.[26] At very short times, $M(t)$ increases linearly with time followed by an "intermediate" time regime when $M(t)$ follows a power law such that $M(t) \sim (t)^{D/6}$ where D is the dimensionality of spatial distribution of the nuclides in the sample that are under observation. Finally, a long-time regime is observed where the recovery of $M(t)$ is exponential in the difference between itself and its equilibrium value. For small concentrations of free electron spins in the sample (a few hundreds of parts per million or less), the power law behavior of $M(t)$ characteristic of the intermediate time regime dominates over wide time intervals.[26] Moreover, it is often not feasible to acquire reliable $M(t)$ data in the short time regime where $M(t)$ is linear in time due to the lack of sufficient signal-to-noise in the spectrum. Hence, for nuclear relaxation via direct dipolar coupling to free electronic spins in a regular, homogeneous three-dimensional solid ($D = 3$), one expects to see the scaling behavior $M(t) \sim (t)^{0.5}$. Consequently, measurement of $M(t)$ for ^{29}Si NMR signals corresponding to various SiC_xO_{4-x} tetrahedral sites in a spin−lattice relaxation experiment presents the opportunity to obtain the dimensionalities of spatial distribution of these sites in the SiOC-PDC structure that can in turn provide important clues to the structural characteristics of these materials at the nanometer length scale. Here, we present the results of a ^{29}Si magic-angle-spinning (MAS) NMR spin−lattice relaxation study of the spatial distribution of SiC_xO_{4-x} tetrahedra in the structure of two amorphous SiOC-PDCs with different O/Si ratios and carbon concentrations.

Experimental Details

Samples Synthesis. Two amorphous SiOC-PDC samples were prepared by thermal treatment of two commercially available polysiloxanes, Wacker-Belsil PMS MK powder, (Wacker-Chemie, Germany) and Polyramics RD-684a (Starfire Inc., USA). For the thermolysis of the samples up to 1100 °C, 1 to 2 g of the polymeric precursor was taken in a quartz crucible. The crucible was then contained in a quartz tube and heated under a steady flow of purified argon (50 mL/min) with a heating ramp of 100 °C/h in a programmable horizontal tube furnace first to 300 °C and was held at this temperature for 1.5 h. Subsequently, the sample was heated at the same rate to the end temperature of

(26) Bodart, J. R.; Bork, V. P.; Cull, T.; Ma, H.; Fedders, P. A.; Leopold, D. J.; Norberg, R. E. *Phys. Rev. B* **1996**, *54*, 15291.
(27) Devreux, F.; Boilot, J. P.; Chaput, F.; Sapoval, B. *Phys. Rev. Lett.* **1990**, *65*, 614.
(28) Sen, S.; Stebbins, J. F. *Phys. Rev. B* **1994**, *50*, 822.

Table 1. ^{29}Si MAS NMR Spectral Simulation Parameters for the Five Si Species in MK1100 and PR1100 Samples

		SiO_4	SiO_3C	SiO_2C_2	$SiOC_3$	SiC_4
MK1100	δ_{iso} (ppm)	-106.8 ± 0.4	-70.93 ± 0.4	-34.41 ± 2.0	5.57 ± 2.3	-10.82 ± 2.9
	fwhm (ppm)	20.64 ± 0.8	25.125 ± 1.6	27.13 ± 3.3	18.08 ± 5.5	19.75 ± 3.7
POLYR-1100	δ_{iso} (ppm)	-107.76 ± 0.2	-70.89 ± 0.2	-33.27 ± 1.0	7.48 ± 1.7	-10.51 ± 0.7
	fwhm (ppm)	22.32 ± 0.5	23.66 ± 1.0	24.69 ± 1.2	28.13 ± 2.2	22.90 ± 2.7

1100 °C and was pyrolyzed. After a holding time of 2 h at the thermolysis temperature, the samples were cooled down to room temperature. Chemical analyses of these two SiOC-PDC samples were carried out at Mikroanalytisches Labor Pascher (Remagen/Germany). Chemical compositions of these two samples can be expressed as $SiO_{1.5}C_{0.68}$ and $SiO_{1.02}C_{4.2}$ with an error bar of ± 0.03 for the stoichiometric coefficients. These two samples will be referred to as MK1100 and PR1100, respectively, in the subsequent discussion. These chemical analyses also indicate the presence of small amounts ($\sim$ 0.1 wt %) of hydrogen in these two samples.

A second sample of MK1100 (MK1100-G) is prepared with Gd^{3+} as a paramagnetic dopant at a concentration level of 0.08 wt % (800 ppm) Gd_2O_3 in order to ensure that the dominant spin−lattice relaxation mechanism for ^{29}Si nuclides is via dipolar flipping with the paramagnetic spins. Relaxation results from this sample are also used to validate the assumption that the same relaxation mechanism is operative in nominally undoped MK1100 and PR1100 samples. This Gd^{3+} doped MK1100-G sample was prepared via modification of a polysilsesquioxane with $Gd(acac)_3$.[29,30] A solution of 40 mg of $Gd(acac)_3$ (Sigma Aldrich) in 5 mL of anhydrous isopropanol was added dropwise to a solution of 2 g of polysilsesquioxane MK Belsil PMS (Wacker, Burghausen, Germany) at ambient temperature. After stirring for 60 min, the solvent was removed in vacuum (10^{-2} mbar). The powder obtained by this process was thermally cross-linked at 200 °C for 1.5 h and subsequently pyrolyzed in argon atmosphere at 1100 °C for 2 h (heating rate 100 °C/h) to yield the MK1100-G sample.

^{29}Si and ^{13}C NMR Spectroscopy. ^{29}Si MAS and $^{13}C(^1H)$ cross-polarization (CP) MAS NMR spectra were collected for all samples using a 7 mm Bruker MAS probe and a Bruker Avance solid-state spectrometer operating at a Larmor frequncey of 99.3 MHz for ^{29}Si and 125.7 MHz for ^{13}C. Crushed samples were taken in ZrO_2 rotors and were spun at a rate of 6 to 7 kHz (± 1 Hz). $^{13}C \leftarrow {}^1H$ CPMAS NMR spectra were collected with a 90° pulse length of 6.5 μs and a ^{1}H spin-locking frequency of 38.5 kHz. A contact time of 1 ms and a recycle delay of 5 s were used. These spectra were collected under two pulse phase modulated (TPPM) proton decoupling[31] with a phase modulation angle of 15° and a pulse duration of 6.5 μs in the proton channel (90° pulse length of 3.65 μs corresponding to an rf field strength of 68.5 kHz). Approximately 15 000 free induction decays were collected and averaged to obtain each ^{13}C CPMAS NMR spectrum.

^{29}Si one-pulse MAS spectra of PR1100 and MK1100 samples were collected using $\pi/3$ (2.6 μs) rf pulses and 60 s recycle delay. Approximately 2000 free induction decays were collected and averaged to obtain each ^{29}Si spectrum. A saturation-recovery pulse sequence was used to measure the spin−lattice relaxation of ^{29}Si nuclides in PR1100, MK1100, and MK1100-G samples.

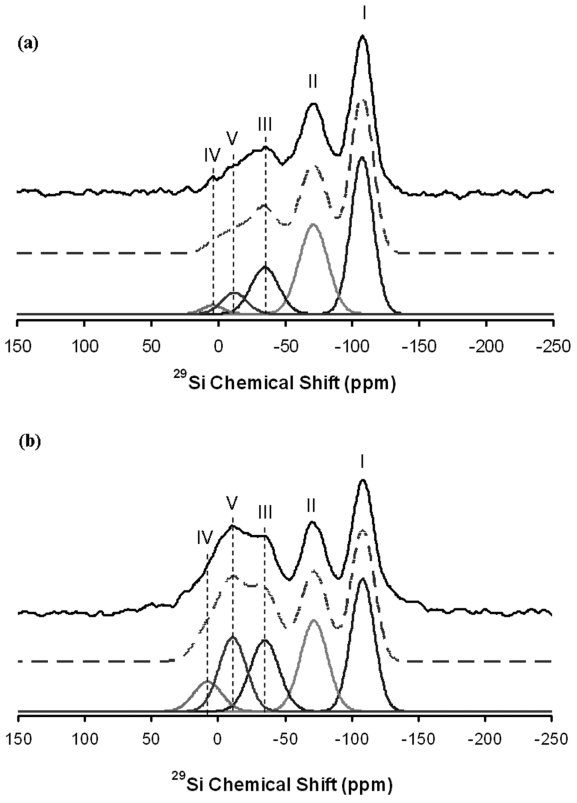

Figure 1. ^{29}Si MAS NMR spectra of (a) MK1100 and (b) PR1100. The experimental spectra are shown by the solid bold line on top, followed by the simulated spectra (dashed lines), and the individual simulation components (thin solid lines). Peak I corresponds to SiO_4 units (−107 ppm), II to SiO_3C units (−70 ppm), III, IV, and V to SiO_2C_2 (−34 ppm), $SiOC_3$ (6 ppm), and SiC_4 (−11 ppm) units, respectively.

A comb of sixteen $\pi/2$ (3.9 μs) rf pulses was used to saturate the magnetization. Free induction decays were recorded after a $\pi/2$ observation pulse at varying delay times ranging from 0.1 to 120 s after saturation. Depending on the delay time, 640 to 7200 free inductions decays were collected and averaged to obtain each ^{29}Si spectrum. All ^{29}Si and ^{13}C NMR chemical shifts were referenced to tetramethylsilane.

All ^{29}Si NMR spectra were simulated with five Gaussian peaks with isotropic ^{29}Si chemical shifts (δ_{iso}) of around −107, −71, −34, 7, and −11 ppm, corresponding respectively to the SiO_4, SiO_3C, SiO_2C_2, $SiOC_3$, and SiC_4 species (vide infra) present in these PDCs (see Table 1). Recovered magnetizations for these silicon species at various delay times after saturation were measured from the areas under the respective peaks. Because of their relatively small amounts and poor signal-to-noise ratio, the relaxation behaviors of the $SiOC_3$ and SiC_4 species have not been considered separately and only an average behavior is reported by combining the corresponding peak areas.

Results

^{29}Si MAS and ^{13}C CPMAS NMR Spectra. The one-pulse ^{29}Si MAS NMR spectra of MK1100 and PR1100

(29) Ionescu, E.; Linck, C.; Fasel, C.; Müller, M.; Kleebe, H.−J.; Riedel, R. *J. Am. Ceram. Soc.* **2010**, *93*, 241.
(30) Ionescu, E.; Papendorf, B.; Kleebe, H.-J.; Poli, F.; Müller, K.; Riedel, R. *J. Am. Ceram. Soc.* **2010**, *93*, 1774.
(31) Bennett, A. E.; Rienstra, C. M.; Auger, M.; Lakshmi, K. V.; Griffin, R. G. *J. Chem. Phys.* **1995**, *103*, 6951.

Table 2. Percentages of Each Si Species As Obtained from ^{29}Si MAS NMR and Corresponding Calculated (NMR) and Analyzed (EA) Chemical Compositions of the MK1100 and PR1100 Samples

	Si species (%)					composition	
sample	SiO_4	SiO_3C	SiO_2C_2	$SiOC_3$	SiC_4	NMR	EA (±0.03)
MK1100	44.0 ± 1.4	30.4 ± 1.1	16.1 ± 1.4	3.0 ± 1.6	6.5 ± 1.1	$SiO_{1.51}C_{0.24}$	$SiO_{1.5}C_{0.68}$
PolyR-1100	32.4 ± 0.7	22.1 ± 0.4	20.6 ± 1.0	8.0 ± 0.2	16.9 ± 1.0	$SiO_{1.23}C_{0.38}$	$SiO_{1.02}C_{4.2}$

samples are shown in Figure 1. Following previous ^{29}Si MAS NMR spectroscopic studies of SiOC-PDCs reported in the literature, these spectra in Figure 1 can be well simulated using five Gaussian peaks with δ_{iso} around −107, −71, −34, 7, and −11 ppm corresponding to the SiO_4, SiO_3C, SiO_2C_2, $SiOC_3$, and SiC_4 structural units, respectively. The relative concentrations of these silicon species obtained from the area under the respective peaks are reported in Table 2. As intuitively expected, the PR1100 sample with high carbon concentration contains higher fractions of carbon-rich SiO_2C_2, $SiOC_3$, and SiC_4 structural units compared to those in the MK1100 sample. These relative concentrations of various silicon species were used to calculate the chemical compositions of the two samples under the assumptions of (1) complete absence of any carbon−oxygen bonds, (2) tetrahedral coordination for Si and C atoms in SiC_xO_{4-x} tetrahedra, and (3) each oxygen being bonded to two Si atoms. These calculated chemical compositions are compared in Table 2 to those obtained from chemical analyses. Such a comparison shows that ∼65 (91) ± 5 atom % carbon in the MK1100 (PR1100) sample is not bonded to silicon atoms and, thus, is present as free carbon that does not belong to the SiOC network.

Representative ^{13}C CPMAS NMR spectra of MK1100 and PR1100 samples are shown in Figure 2. These spectra show four peaks centered at ∼12, 80, 140, and 180 ppm. Spectra collected at different spinning speeds indicate that the peaks at ∼80 and 180 ppm are spinning sidebands of the resonance whose isotropic position is at ∼140 ppm, implying that these three peaks belong to a single carbon environment with a large chemical shift anisotropy (CSA). On the other hand, the resonance with an isotropic chemical shift of ∼12 ppm corresponds to a second carbon site that appears to be substantially more symmetric with significantly smaller CSA compared to the site with isotropic shift of 140 ppm. These ^{13}C CPMAS NMR spectra were, therefore, simulated with two sites, one with a significantly large CSA and the other with zero CSA (Figure 2). These simulations yield the ^{13}C isotropic chemical shifts of 139 (130) and 11 (13) ppm for these two carbon sites with relative fractions of 70 ± 5% (81 ± 5%) and 30 ± 5% (19 ± 5%), respectively, in MK1100 (PR1100). The CSA parameters for the first peak for MK1100 (PR1100) are as follows: span Ω = 151 (172) ppm and skew κ = 0.9 (1.0). The high κ value of ∼1.0 implies that these carbon sites are uniaxially symmetric in both samples, as expected from sp^2-bonded carbon environments in graphite. On the other hand, the Gaussian peak with ^{13}C isotropic chemical shift ranging between 11 and 13 ppm represents a carbon environment with locally cubic site symmetry as in sp^3-bonded carbon sites in SiC.

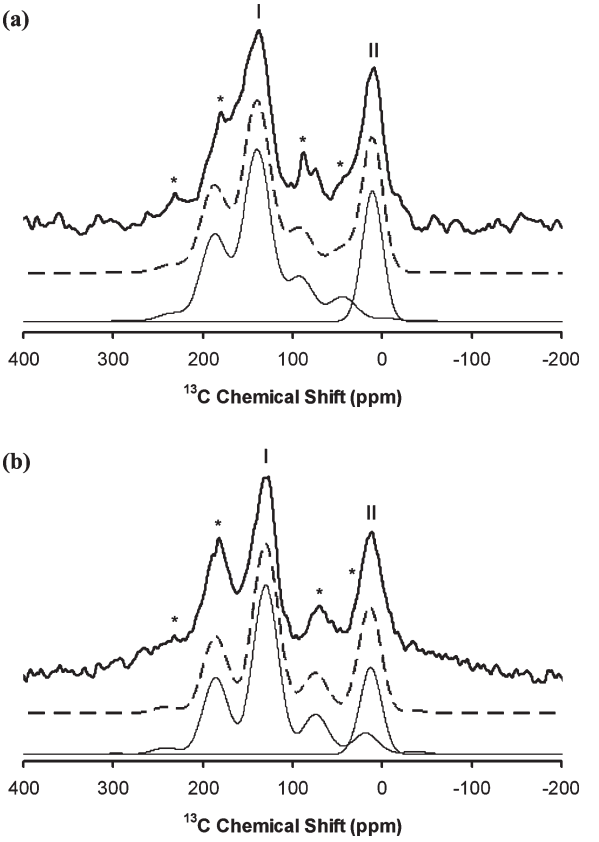

Figure 2. ^{13}C CPMAS NMR spectra of (a) MK1100 and (b) PR1100. The experimental spectra are shown by the solid bold line on top, followed by the simulated spectra (dashed lines) and the individual simulation components (thin solid lines). Peak I corresponds to sp^2 hybridized carbon (∼ 130 ppm), and peak II corresponds to sp^3-hybridized carbidic carbon in CSi_4 sites (∼12 ppm). Peak I is a MAS powder pattern resulting from chemical shift anisotropy (see text for details). Asterisks denote spinning sidebands.

^{29}Si Spin−Lattice Relaxation. The evolution of the ^{29}Si MAS NMR spectra with increasing delay time for MK1100, MK1100-G, and PR1100 samples is shown in Figure 3. Although the ^{29}Si MAS NMR line shapes for the MK1100 and MK1100-G samples are practically identical, the signal-to-noise ratio for similar delay times is significantly higher in the latter sample, implying substantial shortening of the average ^{29}Si spin−lattice relaxation time in this sample due to doping with Gd^{3+}. For all samples, the relative fractions of the various SiC_xO_{4-x} structural units in the spectra are found to remain unchanged within experimental error, regardless of delay times, implying absence of any significant differential relaxation. This relaxation behavior is demonstrated in Figure 4 for the MK1100-G sample.

The widths of the constituent peaks in the ^{29}Si MAS NMR spectra of these SiOC-PDC samples become narrower with increasing delay times, indicating stronger dipolar coupling of the faster relaxing ^{29}Si nuclides that are

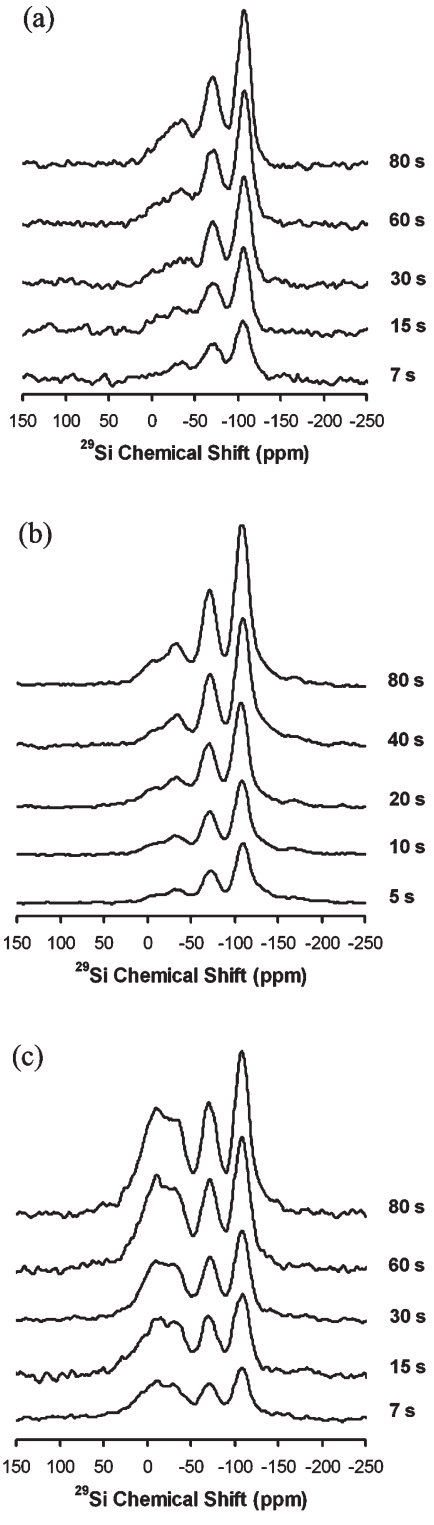

Figure 3. ^{29}Si MAS NMR spectra of (a) MK1100, (b) MK1100-G, and (c) PR1100 obtained at increasing delay times following complete saturation of magnetization. Corresponding delay times are indicated alongside each spectrum.

situated closer to the paramagnetic impurities.[27,28] The recovery of magnetization $M(t)$ with time t for different SiC_xO_{4-x} structural units is shown on a double-logarithmic plot in Figure 5 for all three samples. Long spin−lattice relaxation times, T_1, of ^{29}Si nuclides in these samples prevented the acquisition of the full relaxation curve. However, the linear variation of $M(t)$ in these double logarithmic

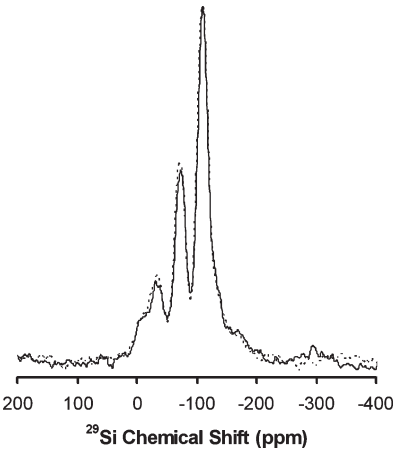

Figure 4. ^{29}Si MAS NMR spectra of MK1100-G sample obtained with delay times of 5 s (solid line) and 40 s (dashed line) following complete saturation of magnetization.

plots over nearly 2 orders of magnitude in time clearly indicates that the recovery of ^{29}Si magnetization for different SiC_xO_{4-x} structural units follows a power law, i.e., $M(t) \sim t^{\alpha}$, as expected in the "intermediate" time regime.[26] As discussed before, the power-law exponent α is expected to be equal to $D/6$ where D is the mass-fractal dimension corresponding to the dimensionality of spatial distribution of the ^{29}Si nuclides around the paramagnetic relaxation centers for each structural unit. The corresponding D values for all SiC_xO_{4-x} structural units are listed in Table 3 for the three SiOC-PDC samples. All D values in Table 3 are significantly smaller than 3 which implies a fractal mass distribution of the constituent structural units and, hence, of the entire SiOC network in these amorphous PDCs, at least at the length scales of ~1−3 nm typically probed by the NMR spin−lattice relaxation experiments.[27,28] The observation of the power law recovery of $M(t)$ also indicates a large distribution of ^{29}Si spin−lattice relaxation times in these samples and, hence, the lack of spin diffusion. Moreover, the fact that the exponential recovery regime for $M(t)$ is still not reached after nearly 100 s of delay indicates that the Gd^{3+} ions are quite widely spaced in the MK1100-G samples (Figure 5b), as expected at such low doping levels of ~800 ppm.

Discussion

The relative concentrations of the SiC_xO_{4-x} structural units in the MK1100 and PR1100 samples are compared in Figure 6 with a statistical model of random mixing of Si−O and Si−C bonds in the SiOC network.[22] According to the latter model, since the oxygen atoms present in the amorphous PDCs would be linked only to two Si atoms, the probability of finding a Si−O bond in the SiOC network p_{Si-O} is one-half of the O/Si atomic ratio, and the probability of finding a Si−C bond p_{Si-C} is given simply by $1 - (p_{Si-O})$. The relative probabilities of finding the SiC_xO_{4-x} structural units are then given by[22]

$$P(SiO_xC_{4-x}) = \frac{4!}{x!(4-x)!}(p_{Si-O})^x(p_{Si-C})^{4-x} \quad (1)$$

The comparison in Figure 6 clearly indicates that for both samples the experimental concentrations of the SiO_4

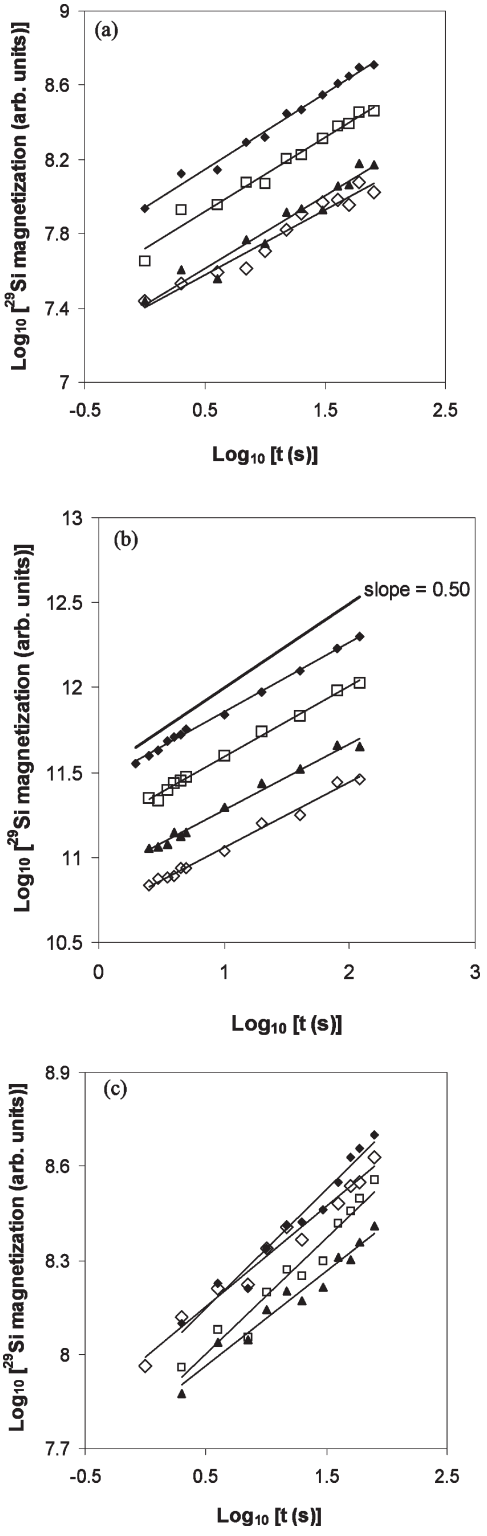

Figure 5. Log of the recovery of the ^{29}Si magnetization for various SiC_xO_{4-x} structural units plotted against the log of the delay time for (a) MK1100, (b) MK1100-G, and (c) PR1100. Magnetization of SiO_4, SiO_3C, SiO_2C_2 and combined magnetization of $SiOC_3$ and SiC_4 species are shown as solid diamonds, open squares, solid triangles, and open diamonds, respectively. Thin solid lines are linear least-squares fits to the data indicating power law recovery of magnetization (see text for details). Thick solid line in (b) with a slope of 0.5, expected from a 3-dimensional spatial distribution of relaxing species, is shown as a reference for comparison.

and SiC_4 units are significantly higher than those expected from a statistical mixing model of Si−O and Si−C

Table 3. Dimensionalities of Spatial Distribution of Various Si Species in MK1100, MK1100-G, and PR1100 Samples

sample	SiO_4	$SiCO_3$	SiC_2O_2	$SiC_3O + SiC_4$
MK1100	2.47 ± 0.03	2.45 ± 0.04	2.35 ± 0.07	2.15 ± 0.19
MK1100-G	2.46 ± 0.02	2.52 ± 0.02	2.34 ± 0.04	2.28 ± 0.10
PR1100	2.50 ± 0.02	2.51 ± 0.02	2.10 ± 0.12	1.95 ± 0.15

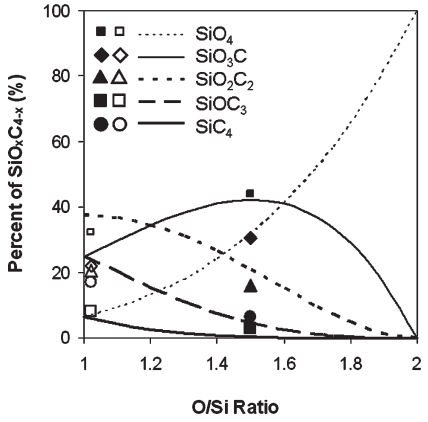

Figure 6. Percentages of various SiO_xC_{4-x} species versus varying O/Si ratio in SiOC-PDCs. Lines show theoretical values corresponding to a statistical model of random mixing of Si−O and Si−C bonds in the SiOC network calculated using eq 1. Percentages of various SiO_xC_{4-x} species in MK1100 with O/Si ∼ 1.5 is shown as filled symbols and in PR1100 with O/Si ∼ 1.02 is shown as open symbols. Explanation of the symbols are given in the inset.

bonds. For example, the expected relative concentrations of SiO_4 and SiC_4 units based on the statistical model in MK1100 (PR1100) samples are 31.64 (6.75)% and 0.4 (5.76)%, respectively, while the observed values from ^{29}Si MAS NMR are 44 (32.4)% and 6.5 (16.9)%, respectively. This result, combined with the observation made in previous studies based on vibrational spectroscopy that there is no carbon−oxygen bonding in the structure,[1] directly implies spatial segregation and clustering of the oxygen-rich and carbon-rich SiC_xO_{4-x} units in the SiOC networks in both samples. Consequently, the carbon-rich SiC_xO_{4-x} units are expected to be segregated at the interface between the oxygen-rich SiC_xO_{4-x} units and the free carbon nanodomains.

The ^{13}C isotropic chemical shifts of carbon sites in various SiC phases have been reported to range between 10 and 25 ppm.[32] Therefore, the Gaussian peak centered at ∼12 ppm in the ^{13}C CPMAS NMR spectra of MK1100 and PR1100 samples (Figure 2) can readily be assigned to tetrahedrally coordinated C atoms bonded to Si in CSi_4 environments in the SiOC network in these PDCs.[32] The isotropic ^{13}C chemical shift of sp^2-bonded carbon sites in a wide variety of carbon materials including ordered graphite, turbostratic carbon, graphene, buckyballs (C_{60}), C_{70}, and carbon nanotubes range between 108 and 150 ppm while that of graphene ranges between ∼123 and 128 ppm.[33−35] Therefore, the

(32) Dybowski, C.; Gaffney, E. J.; Sayir, A.; Rabinowitz, M. J. *Colloids Surf., A* **1996**, *118*, 171.
(33) Pennington, C. H.; Stenger, V. A. *Rev. Mod. Phys.* **1996**, *68*, 855.
(34) Goze-Bac, C.; Latil, S.; Lauginie, P.; Jourdain, V.; Conrad, J.; Duclaux, L.; Rubio, A.; Bernier, P. *Carbon* **2002**, *40*, 1825.
(35) Darmstadt, H.; Roy, C.; Kaliaguine, S.; Xu, G. Y.; Auger, M.; Tuel, A.; Ramaswamy, V. *Carbon* **2000**, *38*, 1279.

carbon site with ^{13}C isotropic chemical shift ranging between 130 and 139 ppm in the ^{13}C CPMAS NMR spectra in Figure 2 can be assigned to sp^2-bonded carbon as in graphite and/or turbostratic carbon that represent the free carbon phase in the structure of MK1100 and PR1100 PDCs. Moreover, the CSA parameters for this carbon site are also consistent with that reported in the literature for graphite (Ω = 178 ppm and κ = 1.0).[35] As noted before, simulations of the ^{13}C CPMAS NMR spectra in Figure 2 indicate that approximately 70 (81) ± 5 atom % carbon in the structure of MK1100 (PR1100) is present as free carbon in graphitic form. It may be noted that intensities in the CPMAS NMR spectra are not always fully quantitative and depend in this case critically on the spatial distribution of protons with respect to the ^{13}C nuclides in the structure. Nevertheless, the estimates of the free carbon content obtained here are quantitatively consistent, within experimental error, with those obtained from the analyses of the ^{29}Si MAS NMR spectra as discussed above.

When taken together, the mass-fractal dimensions of the SiC_xO_{4-x} structural units in MK1100 and PR1100 samples as obtained from the ^{29}Si spin−lattice relaxation results provide important information regarding the structure of SiOC-PDCs at the nanometer length scale. In a scenario where the structure of the SiOC-PDCs can be thought of as a two phase volume percolation problem, where the two phases may correspond to the SiOC network and free carbon, one expects to observe fractal mass distribution of the phases, especially near the percolation threshold. Such a scenario has been shown to be characteristic of the nanometer-scale clustering of structural units in phase separated oxide glasses.[28] For two phase volume percolation, the infinite (percolating) cluster is expected to have a mass-fractal dimension of ~2.6[36] which is indeed similar to that observed in this study (~ 2.5) for the oxygen-rich SiC_xO_{4-x} structural units in MK1100 and PR1100 samples (Table 3). These structural units may phase separate or segregate from carbon-rich SiC_xO_{4-x} structural units due to the bonding constraints associated with the tetrahedral coordination of Si and C atoms, 2-fold coordinated O atoms, CSi_4 environment for carbon atoms in SiC_xO_{4-x} structural units, and avoidance of carbon−oxygen bonding. Therefore, the mass-fractal nature of the oxygen-rich part of the SiOC network results from a frustrated packing of the building blocks, i.e., the SiC_xO_{4-x} structural units, that gives rise to a "Swiss cheese" (or foam)-like spatially continuous or "infinitely percolating" mass-fractal backbone with "voids". However, unlike empty voids in Swiss cheese, these voids in the structure of PDCs are occupied by the graphitic free carbon phase. This structural model is, therefore, consistent with the above-mentioned "model 1" and is schematically shown in Figure 7. It may be noted here that at the nanometer length scale the structure of SiOC-PDCs with high carbon contents such as PR1100 may also contain spatially bicontinuous nanodomains of free carbon and SiC_xO_{4-x} structural units.

(36) Sahimi, M. *Applications of Percolation Theory*; Taylor & Francis: Bristol, PA, 1994.

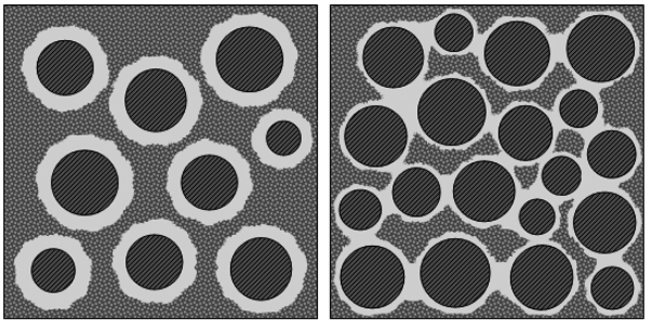

Figure 7. Schematic two-dimensional structural model at the nanometer scale of (a) MK1100 and (b) PR1100. Graphitic carbon nanodomains are shown as dark shaded circles, and the C-rich SiC_xO_{4-x} structural units are shown as light gray regions surrounding these circles. The patterned matrix represents the oxygen-rich SiC_xO_{4-x} structural units forming the fractal backbone.

The observed mass-fractal dimension of ~2.5 for oxygen-rich SiC_xO_{4-x} units is not completely consistent with the presence of isolated silica-rich nanodomains in the structure of SiOC-PDCs, as has been speculated in "model 2". According to percolation theory, the mass-fractal dimension for such finite (i.e., isolated) clusters should be significantly lower than 2.5.[28,36] On the other hand, for dense finite clusters, one expects to observe a dimensionality of 3.

As mentioned above, the nonstatistical mixing of Si−O and Si−C bonds and the absence of any carbon−oxygen bonding in the structure of these SiOC-PDCs imply spatial segregation of oxygen-rich and carbon-rich SiC_xO_{4-x} units. Therefore, the oxygen-rich SiC_xO_{4-x} structural units are expected to be concentrated in the interior of the fractal backbone while the carbon-rich units would be located near and at the interface between this backbone and the free carbon nanodomains. Consequently, the spatial distribution of the carbon-rich SiC_xO_{4-x} units would have a somewhat lower fractal dimension compared to that of the oxygen-rich SiC_xO_{4-x} units in the backbone, especially in highly carbon-rich PDC samples such as PR1100 characterized by large interfacial area. This hypothesis is consistent with observed fractal dimension of ~2.3 and 2.1 for SiC_xO_{4-x} units with $x \geq 2$ in MK1100 and PR1100, respectively (Table 3).

It should be noted here that any difference in the fractal dimensions of SiC_xO_{4-x} units implies corresponding differences in the temporal recovery of magnetization and consequently differential relaxation. Moreover, any inhomogeneity in the spatial distribution of paramagnetic impurities or dopants in the constituent phases in a phase separated structure is also expected to give rise to differential relaxation. Therefore, the above-mentioned lack of any significant differential relaxation in the ^{29}Si MAS NMR spectra of these SiOC-PDCs may imply that such effects are small and lie within experimental uncertainties. Nevertheless, the ^{29}Si spin−lattice relaxation results presented here clearly and unequivocally demonstrate the mass-fractal nature of the SiOC network in SiOC-PDCs with a fractal dimension that is significantly lower than 3. This is expected to give rise to unusual mechanical and transport properties characteristic of fractal percolation

networks. For example, elastic moduli and transport properties such as electrical conductivity and viscosity may show power-law dependence on composition near and above the percolation threshold of the SiOC network or that of the free-carbon phase.[36] Future studies of composition dependence of such properties may, thus, play an important role in understanding the structure−property relationships in this important class of materials.

Summary

The high-resolution ^{29}Si and ^{13}C NMR results, when taken together, suggest that the structure of SiOC-PDCs consists of a network of interconnected SiC_xO_{4-x} structural units that is characterized by a fractal mass distribution with an average dimensionality of $D \sim 2.4$ to 2.5 at length scales on the order of a few nanometers. This fractal network is interspersed with nanodomains of sp^2-hybridized free carbon that is primarily present as graphitic carbon. The Si−O and Si−C bonds in this SiOC network are not homogeneously mixed but clustered. The oxygen-rich SiC_xO_{4-x} structural units with $x < 2$ are expected to be concentrated in the interior of this network while the carbon-rich units with $x \geq 2$ are expected to be located at the interface with the free carbon nanodomains.

Acknowledgment. This study was performed within Materials World Network collaborative project "Nanostructure and thermodynamics of polymer-derived ceramics" and was supported by NSF Grant MWN-0907792. G.M. and R.R. also gratefully acknowledge the financial support by the Fonds der Chemischen Industrie, Frankfurt (Germany).